Journal of Solid State Chemistry **143,** 210–218 (1999)
Article ID jssc.1998.8088, available online at http://www.idealibrary.com on IDEAL®

Crystal Growth and Defect Structure of Al^{3+}-Doped Rutile

U. Gesenhues and T. Rentschler

Sachtleben Chemie GmbH, Laboratories, Postfach 170454, 47184 Duisburg, Germany

Received May 26, 1998; in revised form October 23, 1998; accepted October 27, 1998

Four microcrystalline rutile powders doped with 0–0.8% Al_2O_3/ TiO_2 and grown at 930–980°C from the same precursor material were investigated. By synchrotron X-ray diffraction and Rietveld refinement, unit cell parameters and crystallite sizes were determined. Also, FTIR reflectance spectra were recorded for possible contributions from free electrons and lattice vibrations. With increasing amounts of dopant, cell parameters *a* and *c* decrease steadily while the positional parameter *u* has a maximum value with intermediate amounts. Two rutile lattice vibrations sensitive to oxygen vacancies are steadily weakened, and a vibrational mode of the same symmetry appears that is characteristic of Me–O octahedra in corundum. These results prove that Al_2O_3 is incorporated into the rutile lattice and reveal the defect structure: With low amounts of dopant, Al^{3+} substitutes Ti^{4+} and is charge-compensated by oxygen vacancies, and with large amounts of dopant, Al^{3+} is additionally put on interstitial places. The crystal size of rutile increases with temperature, but is not influenced by Al^{3+} doping. © 1999 Academic Press

Key Words: **titanium dioxide; metal oxides; doping; defect structure; oxygen vacancy; crystal growth; unit cell parameters; lattice vibrations.**

INTRODUCTION

Rutile (TiO_2) and corundum (Al_2O_3) are ionic crystals that have in common a hexagonal packing of oxygen anions and the cations positioned in the octahedral holes between them (1, 2). In corundum the anions are 10 vol% more densely packed than in rutile. So Al_2O_3 should at least be partially soluble in TiO_2:

$$2\ Al_2O_3 \rightarrow 3\ Al'_{Ti} + Al_i^{\bullet\bullet\bullet} + 6\ O_O \qquad [1]$$

(Kröger–Vink notation). One Al^{3+} on a substitutional place and another on a neighboring interstitial place in rutile would form a pair of face-sharing Me–O octahedra, a structural element typical of corundum. However, Al^{3+} differs from Ti^{4+} in size and charge. Several defect structures of Al_2O_3 dissolved in TiO_2 can be imagined to compensate this (3):

$$Al_2O_3 \rightarrow 2\ Al'_{Ti} + 3\ O_O + V_O^{\bullet\bullet} \qquad [2]$$

$$Al_2O_3 \rightarrow 2\ Al_i^{\bullet\bullet\bullet} + 6\,e^- + \tfrac{3}{2}\ O_2 \qquad [3]$$

$$2\ Al_2O_3 + Ti_{Ti} \rightarrow 4\ Al'_{Ti} + Ti_i^{\bullet\bullet\bullet\bullet} + 6\ O_O. \qquad [4]$$

In Eq. [2] the Al^{3+} are thought to be statistically distributed over regular cation sites in the rutile lattice, but not bound to the oxygen vacancy. Instead, they may be located in two neighboring Me–O octahedra sharing an edge, with the oxygen vacancy on the edge. Alternately, one of the two Al^{3+} moves away from the oxygen vacancy to an octahedral hole not occupied in the ideal rutile structure. When the second Al^{3+} is in the neighboring regular Me–O octahedron, a pair of face-sharing Al–O octahedra are formed (4). In Eq. [3], the electrons may move into the conduction band of rutile or reduce Ti^{4+} ions. Equation [4] allows for interstitial Ti, which may be stabilized at high temperatures by entropy effects, although it disturbs the periodicity of electric charges in the lattice of pure rutile massively. Furthermore, it is possible that the defect structure of Al-doped rutile varies with temperature, depending on the heat of the reactions in Eqs. [1]–[4], and also with oxygen partial pressure, if Eq. [3] is involved. However, the intrinsic defect equilibrium of rutile (3)

$$2\ TiO_2 \rightarrow 2\ Ti'_{Ti} + 3O_O + V_O^{\bullet\bullet} + \tfrac{1}{2}\ O_2 \qquad [5]$$

can safely be neglected below 1050°C and oxygen partial pressures above 50 mbar (5, 6).

These questions are of practical relevance, as all commercial rutile white pigments, with 4 million tons produced per year, are doped by Al^{3+} in order to suppress the undesirable photoactivity (7). However, a scientific understanding of this solid-state reaction is still missing (8).

In the past, it has been difficult to prepare Al-doped rutile samples in thermodynamic equilibrium and deduce the prevalent defect structure experimentally (3). Also, there is not yet definite agreement with regard to theoretical

0022-4596/99 $30.00

calculations (9). A solubility of 0.5–1.5 mol% Al_2O_3 in rutile has been determined at 1200–1425°C and been explained by Eq. [1] (10). Also, the unit cell parameter *c* of rutile has been observed to shrink steadily with increasing concentrations of Al_2O_3, while parameter *a* remained constant within the uncertainty of measurements (10). In an early EPR study, Al^{3+} ions were found on substitutional places and partly associated to dimers; however, preparation and composition of the sample are not completely clear (11).

Recently, the influences of Al^{3+} on the growth of TiO_2 microcrystals and the transformation of the anatase to the more stable rutile modification have been investigated in the calcination of metatitanic acid, and rutile powders with 0–0.09 mol% Al_2O_3 dissolved (noncompensating) at 985 ± 55°C have been prepared (8). As equilibrium has been established in these samples for the Al_2O_3 distribution between particle bulk and surface, the same must be true for the defect structure of Al_2O_3 in the bulk. With these low amounts of dopant in the bulk, the assumption of point defects often used in solid-state chemistry is justified, so these samples are suited to test the basics of defect chemistry in binary metal oxides. In the following, two sensitive experimental methods, X-ray diffraction (XRD) and IR lattice vibrational spectroscopy, will be used to determine the defect structure of the samples. Additionally, in the preparation of the samples a retardation of crystal growth was noticed when the amount of Al dopant was large enough to cover the crystals by a monolayer. As this result was gained by indirect methods, it will be corroborated here by the Scherrer method, measuring and evaluating the line width of XRD patterns. Synchrotron radiation, however, was necessary because the crystallites investigated here are larger than 100 nm.

EXPERIMENTAL

Materials

Five microcrystalline TiO_2 powders were investigated that had been prepared by annealing metatitanic acid from Sachtleben Chemie GmbH, Duisburg, at 930–980°C. Prior to calcination, the material had been doped with nominally 0–1.0% Al_2O_3/TiO_2 by mixing with a fine-grained grade of hydrous alumina. Up to 0.8% Al_2O_3 the calcined products contained almost exclusively the rutile phase, with larger amounts of dopant they were a mixture of anatase and rutile. Particle sizes measured in a Joyce–Loebl centrifuge were about 0.4 μm. Only a fraction of the Al dopant was incorporated into the rutile lattice; the rest segregated to the surface of the microcrystalline TiO_2 particles. The investigated samples are listed in Table 1 together with some information on preparation and properties, including the concentrations of Al_2O_3 dissolved in the crystal and deposited at the surface. It can be seen that up to a total amount of dopant of 0.8% Al_2O_3, the concentrations of Al in the bulk (noncompensating) and at the surface are directly proportional. Further details are given in (8).

All samples were mildly deagglomerated in a ball-mill and extracted twice with H_2O to remove calcination additives (alkali, phosphate, sulfate) from the particle surface. For FTIR spectroscopy the samples were used under this condition directly and additionally etched four times with HCl (method described in (8)) to remove Al from the particle surface. Then they were cleared from grit particles by a 100-μm sieve, tempered at 400–450°C overnight to desorb H_2O (12), and stored in a dry weighing glass in the desiccator.

Methods

XRD experiments. These were performed at HASYLAB B2 (synchrotron DESY at Hamburg) at room temperature, using a wavelength λ of 1.246 Å and covering a range of diffraction angles 2θ from 20° to 90° by a step size of 0.008°. Resulting XRD patterns were refined by the Rietveld method, program DBWS-9411 (13), to obtain the cell parameters of rutile and anatase. The interatomic distances and angles in rutile as well as the volumes of the Me–O

TABLE 1
Investigated Samples and Results of X-ray Diffraction

Total Al_2O_3 content (%)	Concentration of Al_2O_3 dissolved in TiO_2 (rest = TiO_2) (mol%)[a]	Surface concentration of Al_2O_3 (mol/m^2)	Calcination temperature (°C)	Rutile content (rest = anatase) (%)	Rutile unit cell parameters						Anatase unit cell parameters			
					a (Å)	e.s.d. (Å)	*c* (Å)	e.s.d. (Å)	*V* (Å^3)	*u*	*a* (Å)	e.s.d. (Å)	*c* (Å)	e.s.d. (Å)
0.045	0.038	0	980	99.5	4.5937	8E-6	2.9588	5E-6	62.4368	0.3082(4)				
0.214	0.059	1.9E-6	930	96.5	4.5935	1E-5	2.9588	8E-5	62.4314	0.3102(4)	3.7842	5E-5	9.5169	8E-4
0.478	0.078	5.1E-6	960	99.0	4.5933	1E-5	2.9586	6E-6	62.4217	0.3101(4)	3.7846	3E-5	9.5129	4E-4
0.793	0.129	9.0E-6	960	96.0	4.5931	1E-5	2.9583	5E-6	62.4100	0.3088(4)	3.7845	2E-5	9.5121	3E-4
0.995	0.285	9.0E-6	960	67.0	4.5932	1E-5	2.9584	8E-6	62.4148	0.3091(6)	3.7844	1E-5	9.5125	1E-4

[a] In all samples 0.038 mol% Al_2O_3 (rest = TiO_2) compensate other aliovalent impurities.

octahedra were calculated from the parameter u of the atomic positions (rutile lattice: tetragonal, space group D_{4h}^{14}-$P4_2/mnm$, Ti(0, 0, 0), O($u, u, 0$)). The estimated standard deviations (e.s.d.) of each parameter in the final cycle were provided in the output file of the refinements. Crystal size d_c was determined by the Scherrer equation from the full width at half maximum W of selected reflections:

$$d_c = K\lambda/(W_S \cos\theta). \quad [6]$$

As the experimental line profiles could be excellently fitted by Lorentzian functions, but not by Gaussians, instrumental broadening W_i and broadening W_S due to finite crystal size add up linearly to W. A powder of LaB_6 (NIST, 15 μm) was used as a reference material to determine W_i as a function of diffraction angle. The observed increase of W_i with 2θ could be fitted by a third-order polynomial. This function was used to calculate W_i for the TiO_2 samples. In Eq. [6], a value of 0.9 was used for K. For a rigorous calculation of the crystal diameter further minor corrections of d_c requiring knowledge of particle shape would be necessary (14).

The fractions of rutile and anatase in the samples are known from the XRD experiments described in (8).

UV–VIS diffuse reflectance spectra. These were taken from hand-pressed disks of the powdered samples in an Ulbricht sphere against $BaSO_4$ as reference material (recording range 300–900 nm, resolution 2 nm, spectrometer Philips PU 8800).

FTIR spectroscopy. This was done using the "Infinity Series FTIR" (ATI Unicam Mattson, Madison, WI) in the wave number range 15,500–200 cm^{-1} (wavelength 0.65–50 μm). Samples were measured in (mainly) diffuse reflectance in the "Collector" cell unit; detectors were Si(red) and InAs for NIR, and DTGS (deuterated triglycine sulfate) for the rest of the IR spectrum. As IR diffuse reflectance spectroscopy of powders is a method still under development (15), details of measurement and evaluation are given in the following.

One gram of sample was pressed to a disk of 13 mm diameter and 3–4 mm thickness, corresponding to 40–55 vol% porosity of the disk. A compression load of 2 t was necessary to produce smooth low-gloss surfaces. For visible light, gloss was 55–65% under an angle of incidence of 60°, measured according to DIN 67530. The pellet was placed in the middle, but out of focus under a large aspherical (ellipsoidal) Al mirror of solid angle 2π. One half of the mirror reflected an incoming divergent beam of IR radiation divergently to the pellet, the other half collected the radiation from the pellet and reflected it convergently into the direction of the detector. No blocker was used to suppress contributions from specular reflection, as this weakens diffuse reflection as well. The optical configuration is equivalent to the "in-plane" system in Fig. 6.4-19 of (15). A sandblasted stainless steel plate was used as calibration standard for 100% diffuse reflectance. NIR (IR and FIR) spectra were accumulated from 512 (128) scans.

For the evaluation of reflectance spectra the Kubelka–Munk theory (15) was applied, as illumination was mainly diffuse and as the pellets had low-gloss surfaces and were porous layers of light-scattering and -absorbing particulate matter. Further arguments are given below. From measured reflectance R the ratio of absorption coefficient K to scattering coefficient S per unit thickness of pellet was calculated:

$$(1 - R)^2/(2R) = K/S;$$

$$S = ((n^2 - 1)/(n^2 + 2))^2 \cdot f\{\text{particle size and packing}\}. \quad [7]$$

The index n of refraction (depending on wavelength) is the same for all samples investigated here, and particle sizes are similar (8). Small variations in particle packing density between samples should not influence R: As K increases with packing density so does S because IR scattering of the TiO_2 pigments investigated here is in the Rayleigh domain where particle agglomeration *enhances* S.

Specular reflection at plane surfaces of homogeneous light-transmitting and -absorbing materials is described by Fresnel's equations. Accordingly, materials show enhanced *reflection* ("Reststrahlen") in spectral regions of *very* strong absorption. Reflection extends from the wavelength of the transversal (TO) to that of the longitudinal optical (LO) mode of oscillation. It has been shown by theory and experiment that in principle this also applies to compact layers of strongly absorbing powders (15, 16). For powders additional absorption bands (Fröhlich, Fuchs–Kliewer, etc.) between TO and LO wavelength due to surface polarization effects are observed (15, 16). On the whole, position and intensity of powder absorption bands are intricately influenced by particle size and shape, aggregation, packing density, and the medium in the pores so that reflectance spectra of powders may look quite different for the same material (15, 16). With inorganic ionic oxides, TO and LO frequencies of the strongest lattice modes are far apart (200/900 cm^{-1}). Between them appear weaker lattice modes with narrow TO/LO spacings, giving dips of absorption in the main reflectivity band (17).

It has been tested that under the experimental conditions used here, the spectral bands observed with powders of pure rutile and anatase as well as α- and γ-Al_2O_3 correspond in number, position, and relative intensity to those of the respective single crystals from literature data. So these conditions were appropriate to our samples of Al-doped TiO_2. With all of them the strongest spectral band at 900 cm^{-1} had the same intensity. For conclusions from the quantitative evaluation of the IR spectra, only the weaker modes are used. Therefore our evaluation by Kubelka–Munk and interpretation of results are on firm ground. Within this

framework, oscillator strengths are still proportional to the areas of absorption bands, but the calculation of absolute values would require a knowledge of S in Eq. [7].

RESULTS

XRD

The quality of Rietveld refinements with our samples is illustrated in Fig. 1. Results for rutile cell parameters a and c and positional parameter u as well as the rutile content of the samples are given in Table 1. Calculated interatomic distances and angles appear in Table 2. Observed changes for a and c are larger by at least one order of magnitude than the refinement e.s.d. values. The determination of positional parameter u is less accurate, as e.s.d. $= 0.0004$ here, but observed changes are still significant. In Table 1, the experimental values of a and c for the TiO_2 sample with the lowest amount Al_2O_3 (dissolved in compensation) coincide well with the values for pure rutile at room temperature (1). It has been proved by further experiments with undoped TiO_2 samples that the atomic positions in TiO_2 always relax to the room temperature values with our conditions of preparation (calcination temperature and rate of cooling afterward). So the changes of a and c observed with our samples in Table 1 are due to Al doping. The results for the sample with 1% Al_2O_3 do not fit into the trend observed with lower amounts of Al_2O_3, however, this sample contains an extraordinarily large fraction of anatase. The solubility of Al_2O_3 in anatase is not known.

For crystal size determination the four strongest reflections of rutile and anatase were examined. The profile broadening measured with LaB_6 in this 2θ-range was of the order 0.02°; with the TiO_2 samples it was in the range of 0.04°. Thus crystal size could be reliably measured. For results see Table 3. There, h, k, l are the Miller indices.

UV-VIS

With all samples, spectra show the normal shape of pure rutile with the absorption edge at the border between UV and VIS and a reflectance independent of wavelength in the VIS range as reported, e.g., in (7). For want of space, illustrations are not given here.

FTIR

In the NIR range absorption increases faintly and steadily down to 4000 cm^{-1}, but does not show an intermediate maximum. Al doping has no effect on the NIR spectrum. In the central IR and FIR range, our TiO_2 samples show a broad medium absorption around 3400 cm^{-1} and a sharp weak absorption at 3695 cm^{-1}, both due to laterally interacting and isolated OH and H_2O adsorbed at the particle surface; further, a very intense absorption at 900 cm^{-1} and other weaker bands below, illustrated in Fig. 2, are observed which are all due to vibrations of the rutile crystal lattice. The assignment of these bands follows from Fig. 3 (1). With the undoped rutile sample, the intensities of the weak bands in Fig. 2 relative to that of the strong band at 900 cm^{-1} correspond to those of spectra given in the literature (17). With increasing amounts of Al dopant, the band at 900 cm^{-1} does not change while the bands at 370 and

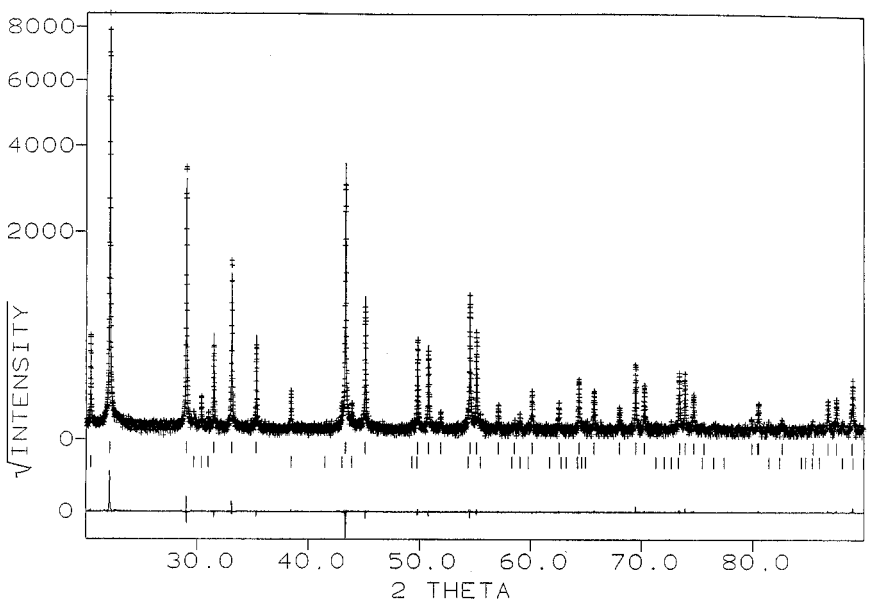

FIG. 1. Rietveld refinement of XRD of the rutile sample doped with nominally 0.8% Al_2O_3: +, experimental values; full line, calculated profile; upper reflection markers, rutile; lower reflection markers, anatase; thin line below, difference profile.

TABLE 2
Calculated Interatomic Distances and Angles of the Rutile Phase from XRD

Total Al_2O_3 content of sample (%):	0.045	0.214	0.478	0.793	0.995
Positional parameter u:	0.3082(4)	0.3102(4)	0.3101(4)	0.3088(4)	0.3091(6)
Distance Ti(1/2, 1/2, 1/2)–O(u, u, 0) (Å):	1.934	1.926	1.926(2)	1.932	1.930
Distance Ti(0, 0, 0)–O(u, u, 0) (Å):	2.002	2.015	2.014(3)	2.006	2.008
Distance O(u, u, 0)–O($1-u$, $1-u$, 0) (Å):	2.492	2.467	2.467(5)	2.484	2.480
Distance O(u, u, 0)–O($1/2+u$, $1/2-u$, 1/2) (Å):	2.784	2.787	2.787(1)	2.784	2.785
Distance O(u, u, 0)–O(u, u, 1) (Å):	2.959	2.959	2.959(0)	2.958	2.958
Angle O(u, u, 0)–Ti(1/2, 1/2, 1/2)–O($1-u$, $1-u$, 0) (°):	80.20	79.63	79.65(12)	80.05	79.94
Angle Ti(0, 0, 0)–O(u, u, 0)–Ti(1/2, 1/2, 1/2) (°):	130.10	129.82	129.83(7)	130.02	129.97
Volume TiO_6 octahedron ($Å^3$)	9.842	9.806	9.801	9.826	9.820

455 cm^{-1} decrease, and a shoulder at 485 cm^{-1} develops to the second band. This corresponds to a strong normal mode of corundum of symmetry E_u (17–19). The contributions of rutile and corundum lattice vibrations to the second band in our samples can be deconvoluted with the help of the spectrum of the undoped rutile sample. The areas of the first band and the deconvoluted second band above the base line provided by the main reflectivity band are given in Fig. 4. They are proportional to the oscillator strengths of the respective modes.

DISCUSSION

Proof of Dissolution of Al_2O_3 in Rutile

The results of XRD in Table 1 show a steady decrease of rutile cell parameters a and c with increasing total amounts of Al dopant. This proves that Al_2O_3 is truly dissolved in increasing concentrations in the rutile lattice. A previous investigation (8) by an indirect method had come to the same conclusion, and the values for the concentrations of dissolved Al_2O_3 determined there can now be safely used. The same is proved by IR spectroscopy: With increasing amounts of dopant the bands at 455 and 370 cm^{-1} lose intensity with respect to the most intense band at 900 cm^{-1}, and the profile of the 455 cm^{-1} band changes; see Fig. 2. These principal changes observed by both methods are bulk phenomena and cannot be caused by changes in the surface chemistry of these microcrystals. Such effects are observed only for much smaller particles (16, 20). However, some minor effects of surface layers have been found in the IR spectra of our samples (see Figs. 2 and 4) and will be discussed below.

TABLE 3
Crystal Size d_c (in nm) Determined from XRD Reflections

		Total Al_2O_3 content (%)					
$h\ k\ l$	2θ (°)	0.045	0.13[a]	0.214	0.478	0.793	0.995
			Rutile				
1 1 0	22.11	262	224	168	185	213	149
1 0 1	29.01	331	270	179	315	261	252
1 1 1	33.10	357	283	174	310	298	218
2 1 1	43.33	410	316	174	311	295	215
			Anatase				
1 0 1	20.41			115	269	227	244
2 0 0	38.45				203	235	274
1 0 5	43.01						201
2 1 1	43.92						219

[a] Linearly interpolated to 960°C, from samples 0.045%, 980°C and 0.214%, 930°C.

Unit Cell Dimensions

In Fig. 5 the relative changes of rutile cell parameters a and c observed with our samples are plotted against the concentration of Al_2O_3 dissolved in rutile. Apparently the unit cell shrinks equally in all three dimensions with these low concentrations. This points to a defect structure that is different from the one around 1300°C, where only a much stronger shrinkage of cell parameter c had been found, but over a much larger range of Al_2O_3 dissolved in rutile (10). In our work the shrinkages $\Delta a/a$ and $\Delta c/c$ are ca. -0.17 per mol Al_2O_3, to be compared with -0.052 per mol Al_2O_3 for $\Delta c/c$ in (10). If defect structure [2] is assumed to prevail in our samples and if the rutile lattice can shrink to the same extent that oxygen vacancies are generated by doping, a concentration of 0.05 mol% Al_2O_3 noncompensating dissolved in rutile would give a shrinkage of the unit cell by 5.0×10^{-2} vol%. The experimental value from Fig. 5 is 2.4 to 2.8×10^{-2} vol%, which is not that different. The difference may be explained by repulsion between the anion electron clouds which grows with lattice shrinkage. With the other defect structures mentioned in the Introduction, cation interstitials are created instead of anion vacancies by doping. Thus the octahedral holes between the anions are

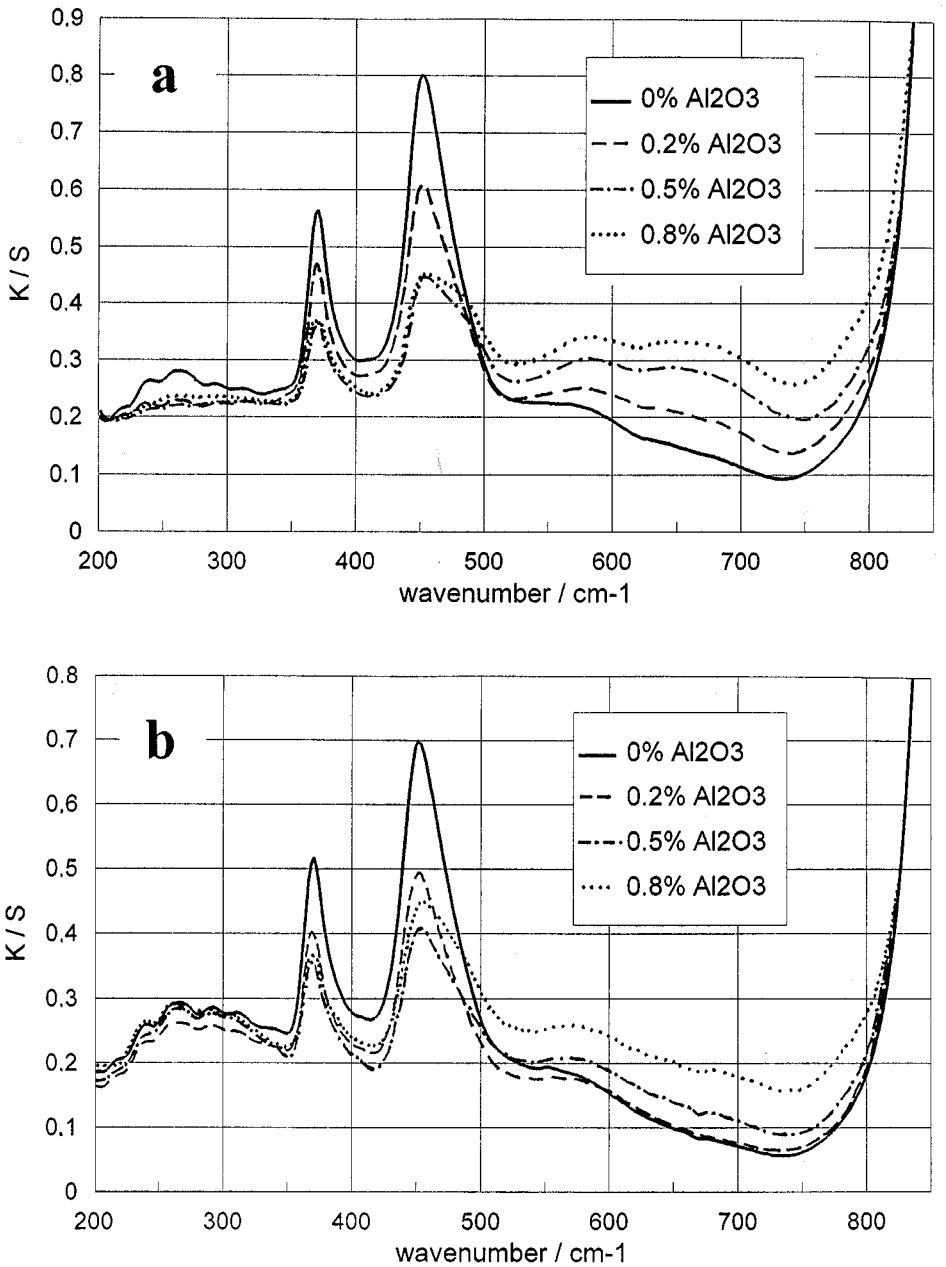

FIG. 2. IR spectra of the Al-doped rutile samples before (a) and after (b) etching with HCl.

filled by cations to a higher percentage than in pure rutile, which increases the contribution of cation–anion attraction to the crystal's cohesive energy. As a consequence, a lattice shrinkage could also be imagined with defect structures [1], [3], and [4].

Interatomic Distances

The distances between oxygen neighbors in rutile fall into three groups, the shortest of which is that of the common edge d_{O-O} of Ti–O octahedra aligned along the c axis. This distance makes the largest contribution of anion electron cloud repulsion to the crystal lattice energy. In Table 2, with increasing amounts of Al dopant d_{O-O} first decreases, then increases. By definition changes of u run into the opposite directions; see Table 1. However, with increasing u the Madelung number grows (21), so the changes in anion electron cloud repulsion with Al doping are compensated by changes in the Coulomb part of the lattice energy. The Ti–O distances in Table 2 vary by 1.2 pm with Al doping.

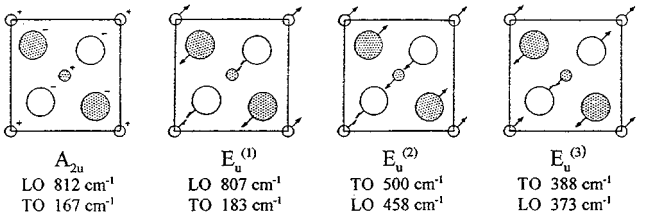

FIG. 3. IR active vibrational modes of rutile (projection drawn down the c axis of the unit cell; small circles, Ti; large circles, O; empty circles, atoms at $c = 0$ and 1; hatched circles, atoms at $c = 1/2$).

Characteristic Lattice Vibrations

In the rutile IR modes of 370 and 455 cm^{-1} two cations (unit cell positions $0,0,0$ and $0,0,1$) vibrate parallel to a third one $(1/2, 1/2, 1/2)$ between them; see Fig. 3. It is evident that the elimination of an oxygen anion between them must extinguish these vibrational modes due to Coulomb repulsion. As this is indeed found with our samples, the effect increasing with the amounts of Al doping, oxygen vacancies are generated in the rutile lattice. The attenuation of these two IR modes has already been observed in the partial reduction of pure rutile, although no conclusions concerning the defect structure have been given (17). Both IR bands are weakened to half of their original intensity already when 0.05 mol% Al_2O_3 are noncompensating dissolved in rutile, i.e., when 1 in 1000 unit cells has one Ti replaced by Al, or when such unit cells are ca. 4 nm apart! With the highest levels of Al doping, the intensities of the two bands do not change further, but a shoulder to one of them develops at 485 cm^{-1}. This is ascribed to the vibration of corundum-type structural elements, i.e., pairs of face-sharing Al–O octahedra, in rutile. This vibration is excited by the 455 cm^{-1} vibration of the rutile surroundings because it has the same symmetry. Since the corresponding mode in pure corundum is as sensitive to oxygen vacancies as that of rutile for the same reason, the 485 cm^{-1} vibration would not be detected in Al-doped rutile if the pairs of Al–O octahedra in rutile contained oxygen vacancies.

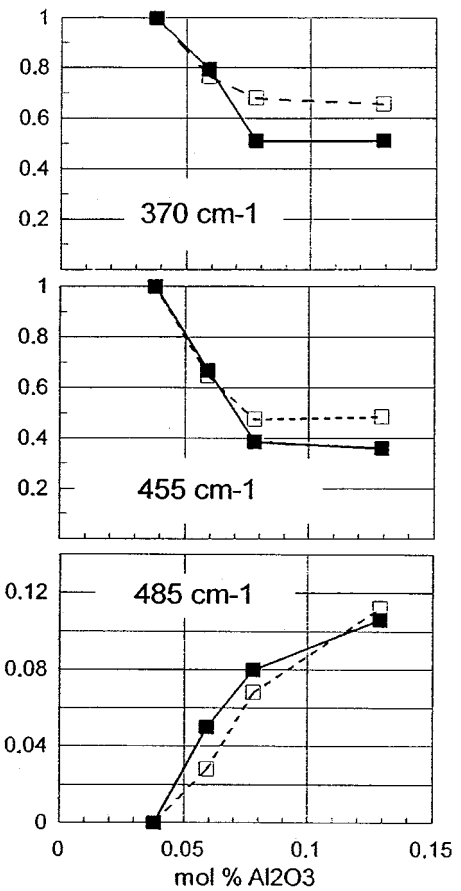

FIG. 4. Peak areas of IR bands, normalized to the values of the undoped sample, against the concentration of Al_2O_3 dissolved in rutile. Full symbols, before, and empty symbols, after etching with HCl.

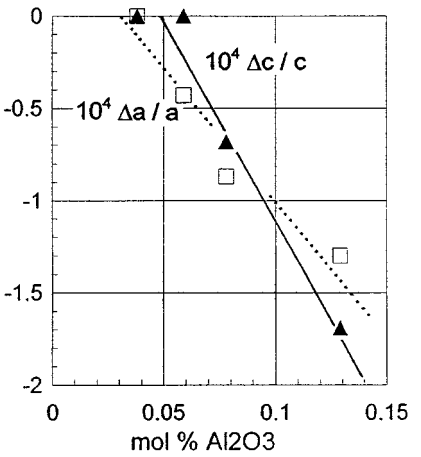

FIG. 5. Relative change of rutile unit cell parameters a (□) and c (▲) with concentration of Al_2O_3 dissolved in rutile.

Defect Structure

According to (7, 22) free electrons in the conduction band of TiO_2 and electrons bound in shallow donor levels give a broad absorption from VIS to NIR with a maximum at 1.24 μm wavelength = 8065 cm^{-1} = 1.0 eV. The reflectance of such a material in the VIS range decreases steadily from 450 to 900 nm. The same decrease should be observed with Al-doped rutile, if defect structure [3] would prevail, and it should be the more prominent the higher the amount of dopant is. However, nothing like that is observed with our Al-doped rutile samples, so defect structure [3] is ruled out. The bidirectional variation of parameter u with increasing amounts of Al doping points to the simultaneous existence of at least two defect equilibria. The structural elements

observed by IR prove defect structure [2] with unreconstructed oxygen vacancies, and with high doping levels additionally defect structure [2] with reconstructed oxygen vacancies or defect structure [1]. Defect structure [2] with unreconstructed oxygen vacancies is also consistent with the growth of u observed in the range of low doping levels: In pure rutile u is small in order to minimize the electron cloud repulsion of the two oxygen anions on the edge shared by two Me–O octahedra (21). If one anion is replaced by a vacancy, this restriction on u is removed. A high value of u is also favorable for the shielding of the cations in these two octahedra against each other. The cation in the third octahedron sharing the oxygen vacancy is always strongly repelled by the two others, no matter which value u takes.

Generally defects in solids begin to cluster when their concentration is raised. With high doping levels a clustering of Al^{3+} is indeed observed in our experiments, but instead of $\{Al'_{Ti} \cdot V_O^{\bullet\bullet} \cdot Al'_{Ti}\}$ it yields $\{Al'_{Ti} \cdot Al_i^{\bullet\bullet\bullet} \cdot V_O^{\bullet\bullet}\}$ or $\{Al'_{Ti} \cdot Al_i^{\bullet\bullet\bullet}\}$. The concentration of $Al_i^{\bullet\bullet\bullet}$ must be proportional to the intensity of the IR band at 485 cm^{-1}, which increases linearly with the amount of Al_2O_3 noncompensating dissolved in TiO_2. The concentration of $V_O^{\bullet\bullet}$ must be proportional to the intensity loss of the bands at 370 or 455 cm^{-1} due to Al doping and reaches a maximum with increasing amounts of Al_2O_3 at 0.04 mol% Al_2O_3 noncompensating dissolved. An argument against Eq. [1] at high doping levels is that the rutile lattice can accommodate oxygen vacancies up to the stoichiometry $TiO_{1.995}$ at ca.1000°C (6). This would correspond to dissolving 0.5 mol% Al_2O_3 according to Eq. [2] in rutile, a level that is not reached in our experiments.

Minor Features in the IR Spectra, Effects of Surface Layers

Between the 455 cm^{-1} band (including shoulder) and the most intense rutile band at 900 cm^{-1} two weak bands are observed with our samples: The band at 570 cm^{-1} is not removed by HCl etching. It may correspond to the Fröhlich surface mode of the two strongest IR-active lattice vibrations of rutile. The second band at ca. 640 cm^{-1} seems to increase with Al doping and disappears by etching. It may be a vibration of the Al_2O_3-like surface layers on the rutile microcrystals derived from a mode in corundum (17–19). The band at 570 or ca. 640 cm^{-1} may also be ascribed to the Raman-active A_{1g} mode of rutile (1, 17) that becomes IR allowed when substitution of Ti^{4+} by Me^{3+}, oxygen vacancies, or Al_2O_3 -like surface layers gives it a polar character. The rutile bands at 370 and 455 cm^{-1} gain intensity when the Al_2O_3-like surface layer is removed; see Figs. 2 and 4. This may be most easily explained when the surface layer consists of an Al-doped rutile defect structure with oxygen vacancies, as proposed in (8), i.e., by the same effect that weakens these bands in the bulk of the crystal by dissolved Al_2O_3.

Crystal Habit

In Table 3, d_c apparently varies with the reflection evaluated, although crystals should be spheroidal according to scanning electron microscopy (8). Thus further contributions to X-ray line broadening have to be considered, although their quantitative separation is beyond the accuracy of our measurements: Compositional inhomogeneities are frequently observed with microcrystals but can be excluded here as d_c does not decrease with increasing diffraction angle (23). Instead, for all samples d_c grows on an average, the effect is least for rutile at 930°C and strongest for rutile at 980°C. This points to lattice strain, according to Warren and Averbach (14) the apparent d_c value should increase with $(h^2 + k^2)$ and with l^2 for tetragonal crystals like rutile and anatase. Then with our rutile samples lattice strain seems to be strong in the direction of c but small in the direction of a. The level of strain does not depend on Al doping, in contrast to the lattice relaxation observed before in a and c. So this strain has probably been induced by ball-milling after calcination. Another source of selective line broadening is anisotropic growth. Microcrystals are on the border where growth may switch from isotropic to oriented, depending on crystal system, impurities, and external conditions. In this intermediate regime, the principal axes of a crystal suffice for a description of growth (20). Thus tetragonal crystals must tend to either needle- or platelike shape or remain spherical, and any direction of growth is fully defined by $x = (h + k)/(h + k + l)$. In view of the effects discussed before, the results in Table 3 show that for the samples investigated here there is no significant indication by XRD for a preferred direction of growth for rutile, and in the sample incompletely transformed to rutile for anatase as well. For rutile, however, the range of x covered here is only from 0.5 to 1.0. In addition, no texture effects could be recognized in the Rietveld refinements. However, when the material doped with 1.0% Al_2O_3 is driven to complete transformation to rutile at higher calcination temperatures, needle-shaped particles appear (8).

Crystal Size

In order to draw conclusions about the effect of Al doping on rutile crystal size, the results in Table 3 must be related to the same calcination temperature for all samples, as crystal growth is accelerated by temperature. The calcination temperatures in Table 1 suggest that we choose a reference temperature of 960°C. So the d_c values measured for 0.045% Al_2O_3 doping, 980°C and 0.214% Al_2O_3, 930°C are interpolated to yield d_c values for 0.13% Al_2O_3, 960°C. The result is given in Table 3. Then the d_c values of the samples doped with 0.13% Al_2O_3 (interpolated), 0.478, 0.793, and 0.995% Al_2O_3 (all measured) can be compared reflection by reflection in Table 3. It follows that the crystal size of rutile

is not influenced by Al doping up to 0.8% Al_2O_3 but decreases with larger amounts of dopant. This confirms the general result of (8) that large amounts of Al^{3+} retard TiO_2 crystal growth, and the value of retardation found here corresponds well to that determined at lower temperatures (8).

CONCLUSION

X-ray diffraction and IR spectroscopy have revealed in which manner Al_2O_3 is incorporated into the rutile lattice under equilibrium conditions: substitutionally in the cation sublattice, with vacancies in the anion sublattice for charge compensation. However, with increasing amounts of dopant, still within the range of applicability of the point defect model, Al^{3+} is additionally set on interstitial sites, which corresponds to the onset of clustering of the Al defect states. Thus they do not repel each other, nor do they cause large lattice strains as a continuous shrinkage of the rutile unit cell with increasing amounts of dopant is possible. So the strong segregation of Al_2O_3 to the surface of rutile crystals observed in (8) must be due to the optimization of lattice and surface energies.

The experimental results concerning the defect structure of Al-doped rutile in this work may set theoretical calculations (Hartree–Fock, density functional, molecular dynamics, etc. (24)) on the right track for a deeper understanding of the effects determining defect structures of metal oxides and their consequences in materials science. The obvious use of lattice vibrational spectroscopy in this work shows that this method may help in the elucidation of other defect structures involving oxygen vacancies and in the determination of the thermodynamics of defect equilibria.

ACKNOWLEDGMENTS

The authors thank Professor A. Reller, University of Hamburg, for providing the experimental facilities of X-ray diffraction at the HASYLAB/DESY. Also the UV–VIS and FTIR spectroscopical work by G. Marten and the department of physicochemical testing at Sachtleben Chemie GmbH is appreciated. The interest of the Sachtleben management in this project is gratefully acknowledged.

REFERENCES

1. O. Madelung (Ed.), "Landolt-Börnstein Zahlenwerte und Funktionen aus Naturwissenschaft und Technik" Gruppe III, Bd.17g. Springer, Berlin, 1984, and quotations therein.
2. C. T. Prewitt, R. D. Shannon, D. B. Rogers, and A. W. Sleight, *Inorg. Chem.* **8,** 1985 (1969).
3. P. Kofstad, "Nonstoichiometry, Diffusion, and Electrical Conductivity in Binary Metal Oxides." Wiley–Interscience, New York, 1972, and quotations therein.
4. L. A. Bursill and M. G. Blanchin, *J. Solid State Chem.* **51,** 321 (1985).
5. J. Nowotny, M. Radecka, and M. Rekas, *J. Phys. Chem. Solids* **58,** 927 (1997).
6. C. Meis and J. L. Fleche, *Solid State Ionics* **101–103,** 333 (1997).
7. U. Gesenhues, *Double Liaison* **43,** No. 479–480, 32 [french version including references], X [english version] (1996), and quotations therein.
8. U. Gesenhues, *Solid State Ionics* **101–103,** 1171 (1997).
9. D. C. Sayle, C. R. A. Catlow, M.-A. Perrin, and P. Nortier, *J. Phys. Chem. Solids* **56,** 799 (1995).
10. R. A. Slepetys and P. A.Vaughan, *J. Phys. Chem.* **73,** 2157 (1969).
11. D. Zwingel, *Solid State Commun.* **20,** 397 (1976).
12. T. Rentschler, *Europ. Coatings J*., No. 10, 939 (1997).
13. R. A. Young, A. Sakthivel, T. S. Moss, and C. O. Paiva-Santos, Program DBWS-9411, 1994.
14. H. Natter, M. Schmelzer, S. Janßen, and R. Hempelmann, *Ber. Bunsenges. Phys. Chem.* **101,** 1706 (1997).
15. B. Schrader (Ed.), "Infrared and Raman Spectroscopy. Methods and Applications." VCH, Weinheim, 1995, and quotations therein.
16. M. Ocaña and C. J. Serna, *Spectrochim. Acta* **47A,** 765 (1991), and quotations therein.
17. J.-F. Baumard and F. Gervais, *Phys. Rev. B* **15,** 2316 (1977), and quotations therein.
18. G. Lucovsky, R. J. Sladek, and J. W. Allen, *Phys. Rev. B* **16,** 5452 (1977), and quotations therein.
19. M. Ashkin, J. H. Parker, Jr., and D. W. Feldman, *Solid State Commun.* **6,** 343 (1968), and quotations therein.
20. A. P. Alivisatos, *in* "XIIIth International Symposium on the Reactivity of Solids." Contribution 2-PL-064, Hamburg, Sept. 8–12, 1996.
21. J. K. Burdett, *Inorg. Chem.* **24,** 2244 (1985), and quotations therein.
22. V. R. Porter, W. B. White, and R. Roy, *J. Solid State Chem.* **4,** 250 (1972), and quotations therein.
23. V. S. Tiwary, N. Singh, and Dh. Pandey, *J. Phys.: Condens. Matter* **7,** 1441 (1995).
24. M. J. Gillan, L. N. Kantorovich, and P. J. D. Lindan, *Curr. Opinion Solid State Mater. Sci.* **1,** 820 (1996), and quotations therein.